



Full paper

A highly-sensitive wave sensor based on liquid-solid interfacing triboelectric nanogenerator for smart marine equipment

Minyi Xu^{a,b,1}, Song Wang^{a,1}, Steven L. Zhang^{b,1}, Wenbo Ding^b, Phan Trung Kien^a, Chuan Wang^a, Zhou Li^c, Xinxiang Pan^{a,d}, Zhong Lin Wang^{b,c,*}

^a Marine Engineering College, Dalian Maritime University, Dalian 116026, China

^b School of Materials Science and Engineering, Georgia Institute of Technology, Atlanta, GA 30332-0245, United States

^c Beijing Institute of Nanoenergy and Nanosystems, Chinese Academy of Sciences, Beijing 100085, China

^d Guangdong Ocean University, Zhanjiang 524088, China

ARTICLE INFO

Keywords:

Wave sensor

TENG

Liquid-solid contact electrification

Electrical double layer

ABSTRACT

Wave monitoring is essential for marine engineering construction, development and utilization of ocean resources, maritime safety and early warning of marine disasters. In this paper, a highly-sensitive wave sensor based on liquid-solid interfacing triboelectric nanogenerator is proposed and systematically investigated. The wave sensor is made of a copper electrode covered by a poly-tetra-fluoroethylene film with microstructural surface. The effects of substrate, wave height, frequency, and water salinity on the performance of wave sensor are systematically investigated. It is found that the output voltage increases linearly with wave height with a sensitivity of 23.5 mV/mm for the electrode width of 10 mm, implying that the wave sensor could sense the wave height in the millimeter range. The sensitivity could be further increased by widening the electrode and/or enhancing the surface hydrophobicity. In a water wave tank, the wave sensor is successfully used to monitor wave around a simulated offshore platform in real time. Therefore, the novel wave sensor could provide an alternative to monitor wave for smart marine equipment.

1. Introduction

Accurate forecasts of wave conditions are essential for marine engineering construction, development and utilization of ocean resources, environmental protection, maritime safety and early warning of marine disasters. There are many types of wave monitoring techniques, such as wave rider buoys, acoustic Doppler current profilers, high frequency radar and remote sensing [1]. Due to each of the techniques has its own advantages and disadvantages, it is essential to choose and develop proper techniques according to the requirements and conditions of applications. These commercial wave monitoring techniques are mainly applied for routine monitoring of waves and currents in the offshore and nearshore regions [2,3]. To enhance the environmental sensing ability of smart marine equipment, it is important to develop a highly sensitive wave sensor to monitor the interaction between ocean waves and marine equipments, such as offshore platforms and ships.

Recently, triboelectric nanogenerator (TENG), based on the coupling of triboelectrification effect and electrostatic induction, has been developed for energy harvesting and for use in self-powered sensors

[4–17]. Its fundamental physics and output characteristics can be attributed to Maxwell's displacement current [18]. As one of the most important types of TENGs, the TENG based on liquid-solid contact electrification has been designed for harvesting water wave energy [19–32], and other applications, such as a self-powered pH [26], concentration [21,33], or pressure sensor [23,34–36]. Zhu et al. proposed and investigated a series of liquid-solid interfacing triboelectric nanogenerator (LS-TENG) for harvesting water wave energy and sensing [19,24,26,28]. These LS-TENGs are made of a fluorinated ethylene propylene (FEP) thin film and an array of copper electrodes underneath, and were used to harvest electrostatic energy arising from liquid-solid interface [19,24–26]. A buoy-like LS-TENG [22], and water tank LS-TENG [20] were also studied for efficiently harvesting water wave energy. A U-shaped LS-TENG was used as self-powered multifunctional sensors, in which the complicated mechanical motions could be transmitted into liquid pressure and electric signal [21,23]. Therefore, the liquid-solid interfacing triboelectric nanogenerator has a great potential to serve as a high sensitive wave sensor for smart marine equipment.

In this paper, a novel wave sensor based on liquid-solid interfacing

* Corresponding author at: School of Materials Science and Engineering, Georgia Institute of Technology, Atlanta, GA 30332-0245, United States.

E-mail address: zhong.wang@mse.gatech.edu (Z.L. Wang).

¹ These authors contributed equally to this work.

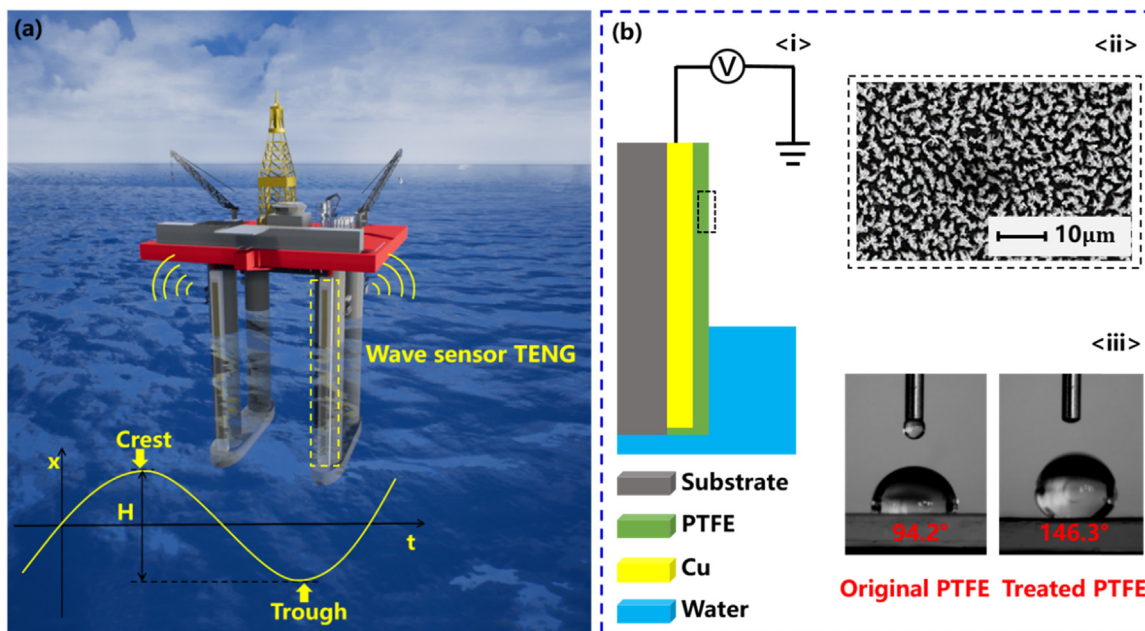


Fig. 1. (a) Schematic diagram of WS-TENG used to monitor waves around a marine equipment. (b) Schematic diagram of the designed WS-TENG. The inset is the scanning electron microscopy image of a treated PTFE surface with microstructure and contact angle measurements of water with original PTFE and treated PTFE.

triboelectric nanogenerator (WS-TENG) is proposed and investigated. The WS-TENG is made of a long copper electrode covered by a polytetrafluoroethylene (PTFE) film with a microstructural surface. The effects of substrate, wave height, frequency, and water salinity on the sensitivity of the wave sensor are experimentally studied and analyzed. In a simulated wave tank, the wave sensor is successfully used for real-time monitoring of the wave around the simulated offshore platform. Therefore, the wave sensor provides an alternative and self-powered approach to monitor waves' characteristics.

2. Results and discussion

2.1. Structure and working principle of the WS-TENG

A schematic diagram of the WS-TENG for monitoring waves around marine equipment, such as a marine platform, is shown in Fig. 1a. The long WS-TENG installed on the legs of the platform can precisely sense the instantaneous water height when ocean waves contact with the WS-TENG surface.

The WS-TENG is comprised of a long rectangular electrode covered by a PTFE film that is attached onto a substrate (Fig. 1b < i >). When an ocean wave interacts with the PTFE surface, there is an electric

potential difference between the copper (Cu) electrode and ground due to the liquid–solid contact electrification, followed by electrostatic induction. To enhance the output voltage of the WS-TENG, the PTFE film was modified by inductively coupled plasma (ICP) etching to obtain a PTFE film with increased surface roughness. The detailed process of the ICP etching is described in the experimental section. The scanning electron microscopy (SEM) image of the treated PTFE surface is shown in Fig. 1b < ii > . The contact angle measurements of water with original PTFE and treated PTFE show the roughness of the film (Fig. 1b < iii >). Therefore, when water contacts with the PTFE, the water would not stay on the PTFE surface, which leaves less water residue on the PTFE surface. Increasing the hydrophobicity implies that the WS-TENG could monitor instantaneous wave height more precisely. In addition, the open-circuit voltage between the Cu electrode and ground is measured for the electrode covered by the treated and original PTFE, respectively. It is found that the treated PTFE film can increase the overall output voltage of the WS-TENG by 63%, compared to that of the original PTFE (Supplementary material Fig. S1). It is also worth noting that the PTFE is the most negatively charged material that is commercially available with respect to triboelectric polarity [37].

The working principle of the WS-TENG is shown in Fig. 2. When

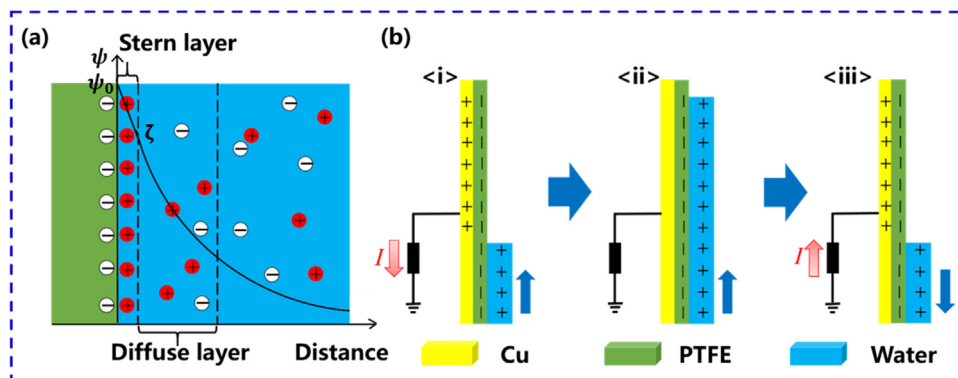


Fig. 2. The working principle of the WS-TENG. (a) The schematic diagram of electrical double layer between water and the PTFE surface of the WS-TENG. (b) The working principle of the WS-TENG and the charge distributed in different stages.

water contacts with the PTFE surface, the surface groups on PTFE may cause its surface to be negatively charged. At the same time, the electrical double layer (EDL) is formed in order to neutralize the charged surface of PTFE and, in turn, causes a potential between the PTFE surface and the liquid [38]. As shown in Fig. 2a, the EDL consists of a Stern layer and a diffuse layer, which are occupied by immobile counterions and mobile ions, respectively [39]. The PTFE surface would retain a negative charge layer that does not dissipate in an extended period of time [38]. When the instantaneous wave height rises (Fig. 2b < i >), positive charges would be induced in the solution to neutralize the negative charges in the PTFE surface; when water leaves the PTFE surface (Fig. 2b < iii >), the same amount of the positive charges would be transferred from the ground to the copper electrode in order to balance the build-up electric field on the PTFE [37]. The amount of the transferred positive charges Q in the electrode is related to the charge density σ_0 and the electrode area S [40], i.e.

$$Q = \sigma_0 S = \sigma_0 wx \tag{1}$$

where σ_0 is the induced charge density and relates to the liquid-solid contact electrification [21,41], and $S = wx$ with w being the width of electrode and x being the instantaneous wave height. This implies that the amount of transferred charges increases linearly with the instantaneous wave height for a WS-TENG working in a solution.

Furthermore, according to the theory of a signal-electrode mode TENG [37], the open-circuit voltage V_{oc} between the electrode (or WS-TENG) and the ground relates to the amount of transferred charges Q , i.e.,

$$V_{oc}(x) = k_q Q(x) = k_q \sigma_0 wx \tag{2}$$

Here, k_q is a correlation factor. From Eq. (2), it implies that the output voltage of the WS-TENG would vary linearly with instantaneous wave height. This is verified in the following experiments by measuring the output voltage of the WS-TENG at different wave height and

frequency. Furthermore, the sensitivity of the WS-TENG $k (= k_q \sigma_0 w)$ may relate to the electrode width and the charge density. Thus, it could be enhanced by widening the electrode and/or enhancing the surface hydrophobicity.

2.2. Performance of the WS-TENG

The dependence of the output voltage V_{oc} of the WS-TENG on substrate, wave height H and wave frequency f is shown in Fig. 3. The WS-TENG is attached onto a substrate connected to a linear motor (Fig. 3a); thus, the device can be driven to move vertically and periodically in a water tank. Note that there is always a part of the WS-TENG that is immersed in the water. The linear motor is programmed to move periodically with $H = 10\text{--}80\text{ mm}$ and $f = 0.6\text{--}1.2\text{ Hz}$. This is essential in measuring the performance of WS-TENG under different wave conditions. To study the effect of the substrate on the performance WS-TENG, the electrical output of the device attached onto the acrylic sheet with different thickness δ and acrylic tube was tested under the same wave condition of $H = 80\text{ mm}$ and $f = 0.6\text{ Hz}$ (Fig. 3a). It is interesting to find that the output voltage peak of WS-TENG increases with the thickness of acrylic sheet varying from 1 mm to 12 mm, and approaches to a constant value for $\delta > 12\text{ mm}$. If the WS-TENG is attached onto an acrylic tube with the thickness of 15 mm, the voltage peak value agrees well with that of the device attached onto the thick acrylic sheet (Fig. 3b). Since there are no charges on the acrylic substrate, due to it is not an electret material, the positive charges on the copper that is induced by the PTFE would be shielded by the water. Thus, the water would be polarized with negative ions facing the copper material on the acrylic side. If the acrylic substrate becomes thicker or is replaced by an acrylic tube with bottom sealed, the thick acrylic or air gap in the acrylic tube could reduce the effect of shielding from the water (Fig. 3b). Even though the transferred charge is the same (Supplementary material Fig. S2), there would be less shielding effect from the water, which

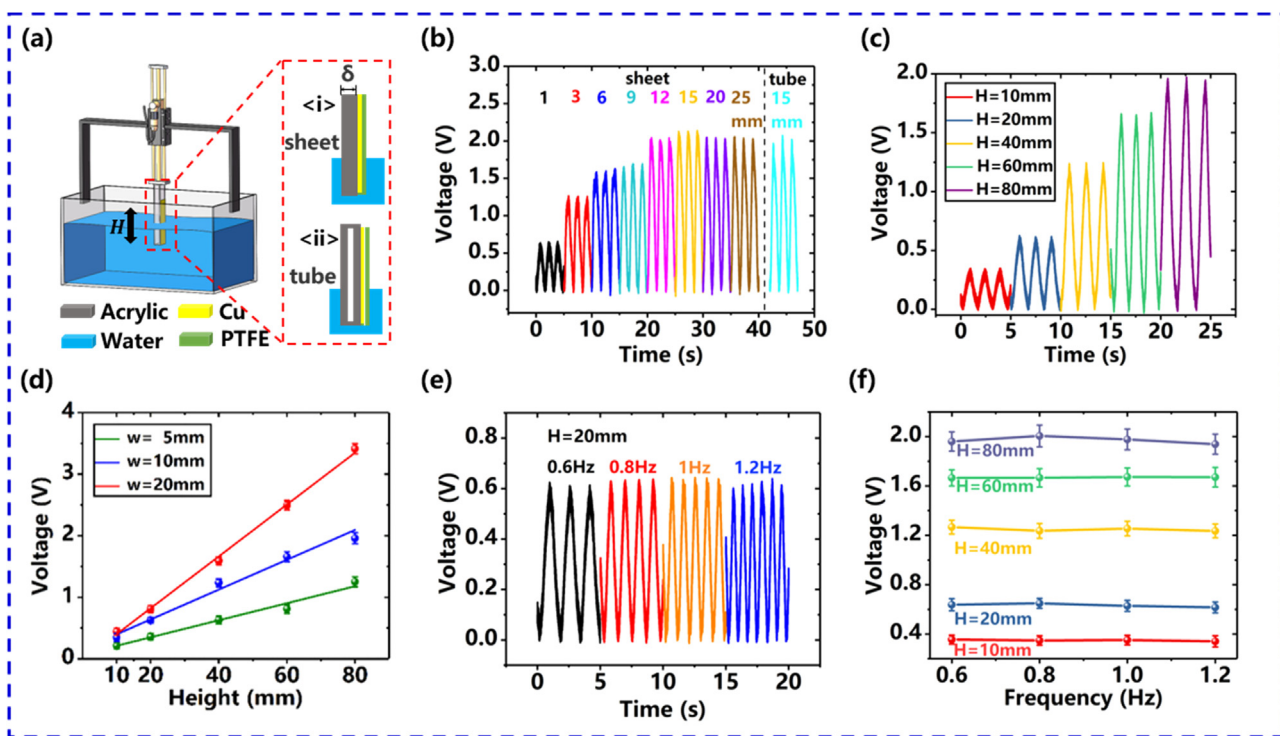


Fig. 3. Dependence of the output voltage of the WS-TENG on substrate, wave height and frequency. (a) Experimental system of the WS-TENG with two types of substrates, i.e., acrylic sheet and acrylic tube. (b) The output voltage of the WS-TENG attached onto the acrylic sheet with different thickness and acrylic tube. (c) The output voltage of WS-TENG with the electrode width of 10 mm measured at $H = 10\text{--}80\text{ mm}$ and $f = 0.6\text{ Hz}$. (d) The relationship between voltage peak value and wave height with $w = 5\text{ mm}$, 10 mm and 20 mm . (e) The output voltage measured at $f = 0.6\text{--}1.2\text{ Hz}$ with the Cu electrode width of 10 mm . (f) Dependence of voltage peak on wave frequency for $H = 10\text{--}80\text{ mm}$.

in turn, cause a higher voltage. This is consistent with the results shown in the previous study [10], and implies that the factor k_q in the Eq. (2) depends on the TENG structure and its working environment. It is also worth noting that the some fundamentals of physical mechanism of the electrical double layer are still elusive [28]; thus, a set of experiments and investigations needs to be performed to establish the theory of the liquid-solid interfacing TENG along with the electrical double layer. In addition, for marine equipment, such as marine platform and ship, the WS-TENG would be attached onto these structure surfaces to reflect the interaction of ocean wave and structure. Thus, the WS-TENG attached onto an acrylic tube with bottom sealed is used as a simulated platform and then systematically investigated as follows.

Fig. 3c shows the output voltage of WS-TENG with the electrode width of 10 mm measured at wave height of 10–80 mm and frequency of 0.6 Hz. The output voltage of the WS-TENG is found to precisely follow the variation of water height. It varies in the frequency of 0.6 Hz and its peak value increases from 0.39 to 1.98 V by increasing wave height from 10 to 80 mm (Fig. 3c). For a wider electrode, the corresponding output voltage increases due to more charges induced on the electrode. The output voltage peaks and their fitting curves are shown in Fig. 3d. The peak value varies linearly with wave height for each WS-TENG. As shown in Fig. 3d, for the WS-TENG with the electrode width of 5, 10 and 20 mm, the fitting relationship of $V_{oc} = kH$ is obtained with the sensitivity $k = 14.1, 23.5$ and 42.5 mV/mm, and a correlation coefficient (R^2) is measured and obtained 0.9797, 0.9816 and 0.9981, respectively. This implies that the WS-TENG could sense the wave height in the millimeter range and the sensitivity could increase by widening the electrode width, while the commercial wave sensors monitor wave height in larger scale range, such as the measurement accuracy of satellite remote sensing technology for wave height is in meter range [1].

Furthermore, the influence of wave frequency on the output voltage of WS-TENG is also studied. Fig. 3e shows the output voltage of WS-TENG under conditions of $f = 0.6$ – 1.2 Hz and $H = 20$ mm. The voltage

vary in the same frequency of water wave, and their peaks are independent of the wave frequency. By extracting and analyzing these peaks, it is found that the voltage peaks' deviation is less than 10% for each wave height (Fig. 3f). This phenomenon is also verified for the WS-TENG with the electrode width of 20 mm (Supplementary material Fig. S3). Therefore, it is concluded that output voltage of WS-TENG varies linearly with the water wave height, but independent of wave frequency.

To study the effect of the salinity on the performance of WS-TENG, the sodium chloride solution was used to simulate seawater with the salinity C varying from 0 to 35 mg mL $^{-1}$. Fig. 4a shows the output voltage of the WS-TENG with $w = 10$ mm under the wave condition of $H = 10$ mm and $f = 0.6$ Hz with varying salt concentration. Obviously, the voltage peak value decreases from 0.35 to 0.15 V when the salinity increases from 0 to 35 mg mL $^{-1}$, suggesting that the sodium chloride solution leads to the rapid reduction of the output voltage of WS-TENG. For higher wave heights, the voltage peak is also found to decrease more dramatically with the salinity increasing from 0 to 35 mg mL $^{-1}$, as shown in Fig. 4b. This supports that the effects of the ionic compounds may be harmful to the output of the liquid-solid interfacing TENG [21]. This phenomenon relates to the liquid-solid contact electrification. With increasing ionic strength, the thickness of the EDL could decrease, leading to a greater number of counter ions electrostatically attached to the dielectric material (e.g., PTFE) surface and, thus, reducing the effective charge Q [39]. Referring to Eq. (2), the less charges transferring between the Cu electrode and the ground would reduce the voltage output of the WS-TENG.

Although the output voltage decreases dramatically with the salinity, it is found to still vary linearly with the wave height (Fig. 4c-d). The curve fitting to these data shows a high linear relationship, i.e., $V_{oc} = kH$, for all solutions. The sensitivity k decreases dramatically as the salinity C increases (Fig. 4e). The relationship $k = a/(C+b)$ with $a = 135.5$ and $b = 5.678$ is obtained by fitting the data. This suggests that the WS-TENG in the solution with high ions concentration could

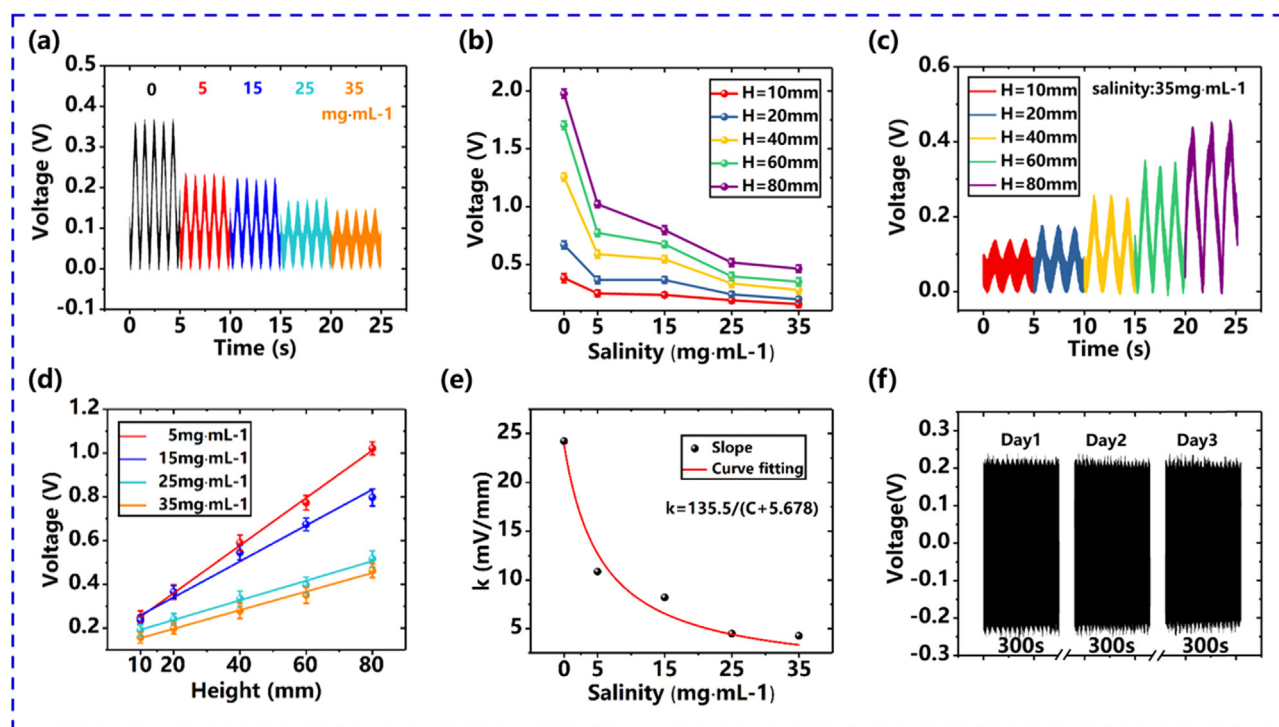


Fig. 4. Effect of salinity on the output voltage and sensitivity of WS-TENG. (a) The output voltage of WS-TENG measured in water with salinity (C) of 0–35 mg mL $^{-1}$ at $H = 10$ mm. (b) Dependence of the output voltage peak on water salinity. (c) The output voltage measured in water with salinity of 35 mg mL $^{-1}$ for $H = 10$ –80 mm and $f = 0.6$ Hz. (d) The relationship between voltage peak value and wave height with salinity of 0–35 mg mL $^{-1}$. (e) The effect of salinity on the sensitivity of WS-TENG. (f) The durability of WS-TENG tested for three days with salinity of 35 mg mL $^{-1}$.

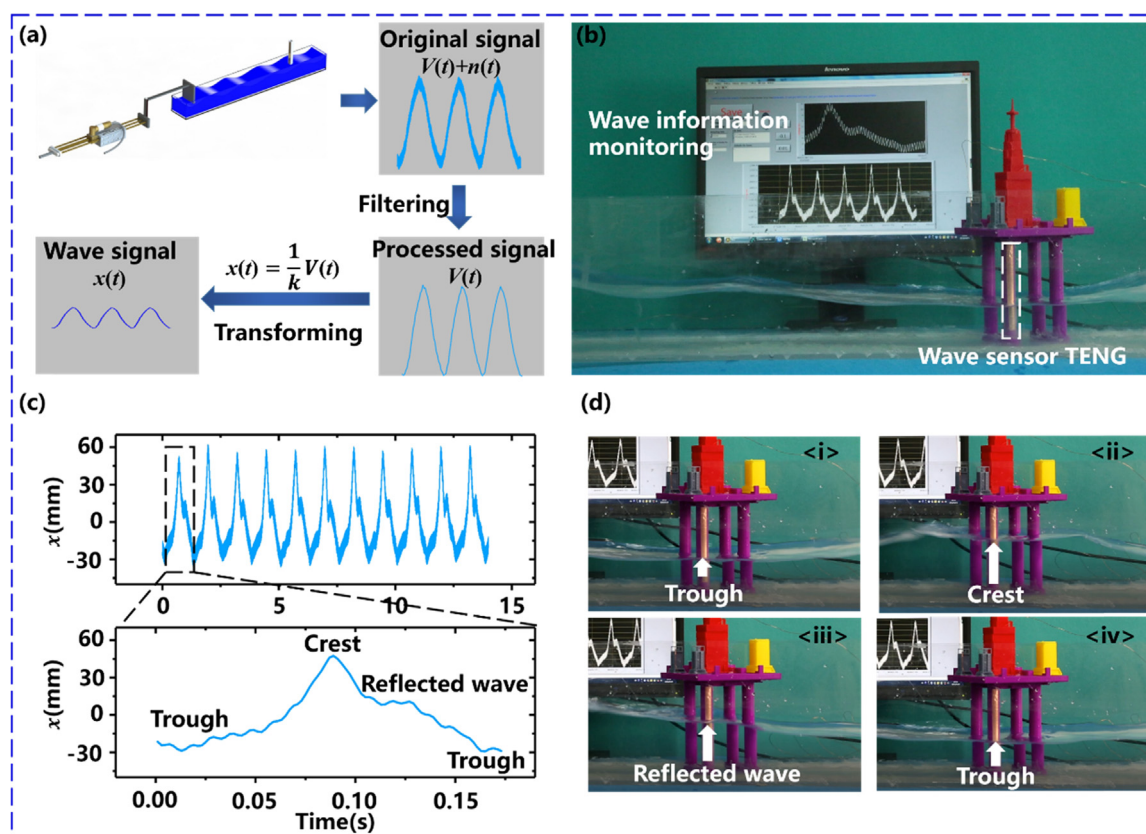


Fig. 5. Applications of the WS-TENG. (a) The process of wave monitoring signals obtained from the WS-TENG. (b) The WS-TENG applied to monitor wave around the leg of a marine platform. (c) The instantaneous wave height x obtained from the WS-TENG. (d) The images of four instantaneous states of water wave in one cycle.

still sense the wave height in the millimeter range. According to Eq. (2), the sensitivity of the WS-TENG would be further enhanced by widening the electrode. In addition, the influence of wave frequency and height on the output voltage peak of the WS-TENG with salinity of 5–25 mg mL⁻¹ is shown in Supplementary material Fig. S4. The output voltage peak of the WS-TENG is obtained and compared at frequencies varying from 0.6 to 1.2 Hz. It is found that the independence of output voltage on wave frequency is also valid for all solutions with different salinity. The output durability of WS-TENG was tested using sodium chloride solution with salinity of 35 mg mL⁻¹ by testing the output voltage over three days. The device output voltage (Fig. 4f) and the microstructures (Supplementary material Fig. S5) in the PTFE surface is consistent over three days, implying the device is durable.

2.3. Demonstration of the WS-TENG

Fig. 5 shows the demonstration of the WS-TENG to monitor waves around a 3D printed offshore platform in a small home-made water tank with 2 m in length, 0.19 m in width and 0.22 m in height. The water wave is generated by a plate driven by a linear motor (Fig. 5a). Here, the plate periodically moves with the linear distance of 120 mm and frequency of 0.8 Hz. It is worth noting that the outside diameter of the 3D printed leg is 20 mm. This would make the back of the WS-TENG does not directly interact with the water, and have the similar role to the thick acrylic sheet or acrylic tube to reduce the effect of shielding from the water; thus, the WS-TENG is directly attached onto the leg of the simulated platform. The original output voltage of the WS-TENG is filtered by a low-pass filter to eliminate noise. Then, the filtered voltage signals $V(t)$ can be converted into instantaneous wave height $x(t)$ by using the relationship $x(t) = V(t)/k$. Here, the sensitivity k for the WS-TENG can be obtained from the fitting relationship between voltage peak value and wave height. When water wave passes over the

platform, the WS-TENG can monitor and record the real-time variation of instantaneous wave height on the leg (see Fig. 5b and Supplementary Video S1). Fig. 5c shows the instantaneous wave height in 11 cycles. From the recorded instantaneous wave height signals, the water wave conditions are obtained with $H = 75$ mm and $f = 0.6$ Hz. In particular, it is worth to note that there is a second peak besides the main peak in one period wave signal. The second peak is caused by the reflected wave from the end of the tank due to the home-made water wave tank being not long enough to dissipate the water wave. Fig. 5d shows the wave patterns passed over the marine platform, i.e., wave valley, wave peak and reflected wave, which are all recorded in the wave signals diagram shown in Fig. 5c. The above data shows that the WS-TENG has great advantages of high-sensitivity to monitor water wave for smart marine equipment. Furthermore, a WS-TENG array made of multiple wave sensors (Supplementary material Fig. S6) could monitor ocean wave information, which can be used by marine scientists, environmental protection agencies, port authorities and the fishing industry.

Supplementary material related to this article can be found online at [doi:10.1016/j.nanoen.2018.12.041](https://doi.org/10.1016/j.nanoen.2018.12.041).

3. Conclusion

In summary, a highly-sensitive wave sensor based on a liquid-solid interfacing triboelectric nanogenerator is proposed and investigated. The wave sensor is made of sensing Cu electrode covered by PTFE film with microstructural surface. The effect of substrate, wave height, frequency and water salinity on the performance of WS-TENG is experimentally studied. It is found that the output voltage peak of WS-TENG varies linearly with wave height. The WS-TENG with the electrode width of 10 mm has a sensitivity of 0.023 V/mm, suggesting that the present novel sensor can sense the wave height in the millimeter range.

The sensitivity would be increased further by widening the electrode, and/or enhancing the surface hydrophobicity. In contrast, the output voltage peak of WS-TENG is independent of wave frequency. Furthermore, the output voltage decays dramatically when water salinity is increased from 0 to 0.035 g mL⁻¹. This may be due to high ions concentration reduces induced charges in electrodes. It is worth to note that the linear relationship between the output voltage of WS-TENG and wave height is still valid at different salinities. In a wave tank, the wave sensor is successfully used to real-time monitor wave around the simulated offshore platform. Therefore, the novel wave sensor has great advantages of high-sensitivity to monitor water wave for smart marine equipment.

4. Experimental section

4.1. Fabrication of the WS-TENG

The WS-TENG was fabricated by first preparing long rectangular copper electrodes with the width of 5 mm, 10 mm and 20 mm and the length of 100 mm. Each electrode completely covered with a 50 μm-thick PTFE tape (from ASF-110FR) and was attached onto a substrate. There are two types of substrates for the WS-TENG, i.e., the acrylic sheet and acrylic tube. The thickness of acrylic sheet varies from 3–25 mm, and the size of acrylic tube is 15 mm in side length, 25 mm in width and 100 mm in height. The bottom of the acrylic tube is sealed to prevent water entering the tube. To enhance the surface hydrophobicity and charge density, the PTFE film was etched through the inductively coupled plasma (ICP) reactive ion etching for 300 s. The reaction gas is 15.0 sccm Ar, 10.0 sccm O₂ and 30.0 sccm CF₄ in the ICP process.

4.2. Electrical measurement of the WS-TENG

The output voltage of the WS-TENG was measured by a programmable electrometer (Keithley Model 6514). To measure the electrical performance of the WS-TENG under different wave conditions, a linear motor (Lin mot E1100) was used to drive the waver sensor to move periodically with the amplitude of 10–80 mm and frequency of 0.6–1.2 Hz. Note that there is always a part of the wave sensor that is immersed in the water. In the demonstration of WS-TENG, a small home-made water wave tank was fabricated with the size of 2 m in length, 0.19 m in width and 0.22 m in height. The linear motor (Lin mot E1100) was also used to drive a plate to generate water wave. The amplitude and frequency for the plate is set to be 120 mm and 0.8 Hz, respectively.

Acknowledgements

The supports of the National Natural Science Foundation of China (Nos. 51879022, 51506019), the National Key Research and Development Program of China (No. 2016YFA0202704), the “Thousands Talents” program for pioneer researcher and his innovation team in China, the Fundamental Research Funds for the Central Universities, China (Nos. 3132016337, 3132016204) and Young Elite Scientists Sponsorship Program By CAST (2016QNRC001) are gratefully acknowledged. Thanks for Dr. Yi-Cheng Wang’s discussion.

Conflict of interest

The authors declare no conflict of interest.

Appendix A. Supporting information

Supplementary data associated with this article can be found in the online version at [doi:10.1016/j.nanoen.2018.12.041](https://doi.org/10.1016/j.nanoen.2018.12.041).

References

- [1] P.K. Pandian, O. Emmanuel, J.P. Ruscoe, J.C. Side, R.E. Harris, S.A. Kerr, C.R. Bullen, *Oceanogr. Mar. Sci.* 1 (1) (2010) 001–010.
- [2] M.C. Marimon, G. Tangonan, N.J. Libatique, K. Sugimoto, *IEEE Syst. J.* 9 (2015) 292–302.
- [3] A.V. Babanin, P.P. Verkeev, B.B. Krivinsky, V.G. Proshchenko, *Phys. Oceanogr.* 4 (1993) 399–407.
- [4] J. Bae, J. Lee, S. Kim, J. Ha, B.S. Lee, Y. Park, C. Choong, J.B. Kim, Z.L. Wang, H.Y. Kim, J.J. Park, U.I. Chung, *Nat. Commun.* 5 (2014) 4929.
- [5] L. Xu, T. Jiang, P. Lin, J.J. Shao, C. He, W. Zhong, X.Y. Chen, Z.L. Wang, *ACS Nano* 12 (2018) 1849–1858.
- [6] T.X. Xiao, X. Liang, T. Jiang, L. Xu, J.J. Shao, J.H. Nie, Y. Bai, W. Zhong, Z.L. Wang, *Adv. Funct. Mater.* (2018) 1802634.
- [7] Z.L. Wang, T. Jiang, L. Xu, *Nano Energy* 39 (2017) 9–23.
- [8] M.-L. Seol, S.-B. Jeon, J.-W. Han, Y.-K. Choi, *Nano Energy* 31 (2017) 233–238.
- [9] L. Jin, W. Deng, Y. Su, Z. Xu, H. Meng, B. Wang, H. Zhang, B. Zhang, L. Zhang, X. Xiao, M. Zhu, W. Yang, *Nano Energy* 38 (2017) 185–192.
- [10] S.L. Zhang, M. Xu, C. Zhang, Y.-C. Wang, H. Zou, X. He, Z. Wang, Z.L. Wang, *Nano Energy* 48 (2018) 421–429.
- [11] M. Xu, P. Wang, Y.-C. Wang, S.L. Zhang, A.C. Wang, C. Zhang, Z. Wang, X. Pan, Z.L. Wang, *Adv. Energy Mater.* 8 (2018) 1702432.
- [12] M. Xu, Y.-C. Wang, S.L. Zhang, W. Ding, J. Cheng, X. He, P. Zhang, Z. Wang, X. Pan, Z.L. Wang, *Extrem. Mech. Lett.* 15 (2017) 122–129.
- [13] S.L. Zhang, Y.-C. Lai, X. He, R. Liu, Y. Zi, Z.L. Wang, *Adv. Funct. Mater.* 27 (2017) 1606695.
- [14] H. Askari, A. Khajepour, M.B. Khamesee, Z. Saadatnia, Z.L. Wang, *Nano Today* 22 (2018) 10–13.
- [15] L. Jin, J. Chen, B. Zhang, W. Deng, L. Zhang, H. Zhang, X. Huang, M. Zhu, W. Yang, Z.L. Wang, *ACS Nano* 10 (2016) 7874.
- [16] B. Zhang, L. Zhang, W. Deng, L. Jin, F. Chun, H. Pan, B. Gu, H. Zhang, Z. Lv, W. Yang, *ACS Nano* 11 (2017) 7440.
- [17] B. Zhang, J. Chen, L. Jin, W. Deng, L. Zhang, H. Zhang, M. Zhu, W. Yang, Z.L. Wang, *ACS Nano* 10 (2016) 6241–6247.
- [18] Z.L. Wang, *Mater. Today* 20 (2017) 74–82.
- [19] X.J. Zhao, S.Y. Kuang, Z.L. Wang, G. Zhu, *ACS Nano* 12 (2018) 4280–4285.
- [20] X. Yang, S. Chan, L. Wang, W.A. Daoud, *Nano Energy* 44 (2018) 388–398.
- [21] L. Pan, J. Wang, P. Wang, R. Gao, Y.-C. Wang, X. Zhang, J.-J. Zou, Z.L. Wang, *Nano Res.* 11 (2018) 4062–4073.
- [22] X. Li, J. Tao, X. Wang, J. Zhu, C. Pan, Z.L. Wang, *Adv. Energy Mater.* 8 (2018) 1800705.
- [23] X. Zhang, Y. Zheng, D. Wang, F. Zhou, *Nano Energy* 40 (2017) 95–106.
- [24] Y. Su, X. Wen, G. Zhu, J. Yang, J. Chen, P. Bai, Z. Wu, Y. Jiang, Z. Lin Wang, *Nano Energy* 9 (2014) 186–195.
- [25] Z.H. Lin, G. Cheng, L. Lin, S. Lee, Z.L. Wang, *Angew. Chem.* 52 (2013) 12545–12549.
- [26] Y. Wu, Y. Su, J. Bai, G. Zhu, X. Zhang, Z. Li, Y. Xiang, J. Shi, *J. Nanomater.* 2016 (2016) 1–6.
- [27] B.D. Chen, W. Tang, C. He, C.R. Deng, L.J. Yang, L.P. Zhu, J. Chen, J.J. Shao, L. Liu, Z.L. Wang, *Mater. Today* 21 (2018) 88–97.
- [28] G. Zhu, Y. Su, P. Bai, J. Chen, Q. Jing, W. Yang, Z.L. Wang, *ACS Nano* 8 (2014) 6031.
- [29] D. Choi, D.W. Kim, D. Yoo, K.J. Cha, M. La, D.S. Kim, *Nano Energy* 36 (2017) 250–259.
- [30] J. Chen, J. Yang, Z. Li, X. Fan, Y. Zi, Q. Jing, H. Guo, Z. Wen, K.C. Pradel, S. Niu, *ACS Nano* 9 (2015) 3324–3331.
- [31] Q. Jing, G. Zhu, P. Bai, Y. Xie, J. Chen, R.P.S. Han, Z.L. Wang, *ACS Nano* 8 (2014) 3836–3842.
- [32] G. Zhu, J. Chen, T. Zhang, Q. Jing, Z.L. Wang, *Nat. Commun.* 5 (2014) 3426.
- [33] Z. Li, J. Chen, J. Zhou, L. Zheng, K.C. Pradel, X. Fan, H. Guo, Z. Wen, M.H. Yeh, C. Yu, *Nano Energy* 22 (2016) 548–557.
- [34] P. Bai, G. Zhu, Q. Jing, J. Yang, J. Chen, Y. Su, J. Ma, G. Zhang, Z.L. Wang, *Adv. Funct. Mater.* 24 (2015) 5807–5813.
- [35] H. Guo, J. Chen, M.H. Yeh, X. Fan, Z. Wen, Z. Li, C. Hu, Z.L. Wang, *ACS Nano* 9 (2015) 5577–5584.
- [36] J. Yang, J. Chen, Y. Su, Q. Jing, Z. Li, F. Yi, X. Wen, Z. Wang, Z.L. Wang, *Adv. Mater.* 27 (2015) 1316–1326.
- [37] Z.L. Wang, L. Lin, J. Chen, S. Niu, Y. Zi, *Triboelectric Nanogenerators*, Springer, Berlin, 2016.
- [38] G. Zhu, Y. Su, P. Bai, J. Chen, Q. Jing, W. Yang, Z.L. Wang, *ACS Nano* 8 (2014) 6031–6037.
- [39] C. Hughes, L.-H. Yeh, S. Qian, *J. Phys. Chem. C* 117 (2013) 9322–9331.
- [40] S. Niu, Y. Liu, S. Wang, L. Lin, Y.S. Zhou, Y. Hu, Z.L. Wang, *Adv. Mater.* 25 (2013) 6184–6193.
- [41] R. Kant, M.B. Singh, *Phys. Rev. E* 88 (2013) 052303.



Minyi Xu received his Ph.D. degree from Peking University in 2012. During 2016–2017, he joined Professor Zhong Lin Wang's group at Georgia Institute of Technology. Now he is an Associate Professor in the Marine Engineering College, Dalian Maritime University. His current research is mainly focused on the areas of blue energy, self-powered systems, triboelectric nanogenerators and its practical applications in smart ship and ocean.



Chuan Wang received the M.S. and Ph.D. degrees from Marine Engineering College, Dalian Maritime University, China, in 2009 and 2012, respectively, both in Marine Engineering. He is currently an Associate Professor with Marine Engineering College, Dalian Maritime University, China. His current research interests include Differential Evolution algorithm, Particle Swarm Optimization algorithm, and Triboelectric Nanogenerators.



Song Wang is currently pursuing his master degree in Dalian Maritime University, China. His research focuses on liquid-solid interfacing triboelectric nanogenerator for energy harvesting and self-powered sensors.



Zhou Li is a Professor and Principal Investigator of Beijing Institute of Nanoenergy and Nanosystems (BINN) and School of Nanoscience and Technology, University of Chinese Academy of Sciences. He is also the director of Nanoenergy and Biosystem Lab in BINN. His research focused on self-powered medical electronics, implantable triboelectric nanogenerator (iTENG), bioabsorbable energy harvester, biosensors and wearable medical devices. He was supported by the National Youth Talent Support Program and award “Young Investigator's Award” by International Federation for Medical and Biological Engineering (IFMBE).



Steven Zhang received his B.S. degree in Electronic Materials Engineering from U.C. Davis in 2014. He is currently pursuing a Ph.D. in Material Science and Engineering at Georgia Institute of Technology, and is working for Professor Zhong Lin Wang. His research focuses on nanogenerators, energy harvesting, and self-powered active sensing.



Xinxiang Pan received his B.E and Ph.D. degrees from Marine Engineering College, Dalian Maritime University, China, in 1987 and 1999. He now is President of Guangdong Ocean University. His research interests include smart and green ship, ocean engineering, energy saving and emission reduction, ship safety and pollution control, microfluidic chip, nano energy and self-powered systems.



Wenbo Ding received the B.E and Ph.D. degrees (highest honors) from the Department of Electronic Engineering, Tsinghua University, Beijing, China, in 2011 and 2016, respectively. He is now a postdoctoral fellow at Georgia Tech, Atlanta, GA, working with Professor Z. L. Wang. His research interests include self-powered sensors, energy harvesting, human-machine interface with the help of signal processing and machine learning. He has received many prestigious awards, including the IEEE Scott Helt Memorial Award, the Tsinghua Top Grade Scholarship (highest honor in Tsinghua), the Excellent Ph.D. Graduate of Beijing City, and the Excellent Doctoral Dissertation of Tsinghua University.



Zhong Lin Wang received his Ph.D. from Arizona State University in physics. He now is the Hightower Chair in Materials Science and Engineering, Regents' Professor, Engineering Distinguished Professor and Director, Center for Nanostructure Characterization, at Georgia Tech. Dr. Wang has made original and innovative contributions to the synthesis, discovery, characterization and understanding of fundamental physical properties of oxide nanobelts and nanowires, as well as applications of nanowires in energy sciences, electronics, optoelectronics and biological science. His discovery and breakthroughs in developing nanogenerators established the principle and technological road map for harvesting mechanical energy from environment

and biological systems for powering personal electronics. His research on self-powered nanosystems has inspired the worldwide effort in academia and industry for studying energy for micro-nano-systems, which is now a distinct disciplinary in energy research and future sensor networks. He coined and pioneered the field of piezotronics and piezophotonics by introducing piezoelectric potential gated charge transport process in fabricating new electronic and optoelectronic devices. Details can be found at: <http://www.nanoscience.gatech.edu>.



Phan.T. Kien received the B.S. degree in Marine Engineering in Vietnam Maritime University, Vietnam, in 2015. He is currently pursuing the Ph.D. degree at the Dalian Maritime University, Dalian, China. His current research interests are triboelectric nanogenerators and their application to ocean wave energy harvesting.